Journal of Material Cycles and Waste Management (2023) 25:1719–1731
https://doi.org/10.1007/s10163-023-01646-3

ORIGINAL ARTICLE

Mechanical properties and microstructure of ground granulated blast furnace slag-based geopolymer reinforced with polyvinyl alcohol fibers

Ting Yu[1,2] · Jiarong Chen[1,2] · Haozhe Guo[3] · Baifa Zhang[4] · Xibin He[5] · Anmin Zheng[5] · Qiang Wang[6] · Peng Yuan[1,7]

Received: 12 October 2022 / Accepted: 7 March 2023 / Published online: 19 March 2023

Abstract
Ground granulated blast furnace slag (GGBFS) is a solid waste characterized by a high reactivity with alkali solutions, which is normally used geopolymer precursor. Fiber is often used to reinforce geopolymer. However, systematic investigation on the relationship between mechanical properties and microstructure for PVA fibers reinforced GGBFS-based geopolymer (FRGp) is neglected. In this study, the effects of the PVA fiber content on the mechanical properties and microstructure of the geopolymer were investigated. The incorporation of PVA fibers into the Gp reduced its compressive strength, attributable to the increase in pore size and total porosity from 4.0% to 7.6%. Nonetheless, the PVA fibers could confine the crack propagation and absorb energy, thereby remarkably increasing the flexural strength of the FRGp. The FRGp containing 2.0 wt% PVA fibers exhibited a flexural strength of 10.1 MPa, 65.6% higher than the Gp after 28 days of curing. Moreover, the PVA fibers exhibited strong physical adhesion to the geopolymer matrix without altering its mineral composition. The results of this study can further elucidate that PVA fibers can pose the positive and negative effects on flexural strength and compressive strength based on the microstructure, respectively, which provided some basic theories for the practical application of Gp.

Keywords Ground granulated blast furnace slag (GGBFS) · Polyvinyl alcohol (PVA) fibers · Fiber-reinforced geopolymer · Mechanical properties · Microstructure

Introduction

Ground granulated blast furnace slag (GGBFS) is a byproduct of steel manufacturing. It is generated through the water-quenching of molten iron ore furnace slag and then grounding to the required fineness. GGBFS mainly consists of calcium oxide, silica, alumina, and magnesia, as well as some other oxides in small quantities [1].

GGBFS, a common solid waste from steel manufacturing, is widely distributed and generated in high yield. The production of 1 ton of pig iron is expected to yield 200–400 kg of liquid GGBFS and the annual global output reaches approximately 270–320 million tons [2–4].

✉ Haozhe Guo
guohaozhe@grre.gd.cn

1 CAS Key Laboratory of Mineralogy and Metallogeny/ Guangdong Provincial Key Laboratory of Mineral Physics and Materials, Guangzhou Institute of Geochemistry, Institutions of Earth Science, Chinese Academy of Sciences, Guangzhou 510640, China

2 University of Chinese Academy of Sciences, Beijing 100049, China

3 Institute of Resources Utilization and Rear Earth Development, Guangdong Academy of Sciences, Guangzhou 510650, China

4 School of Civil and Transportation Engineering, Guangdong University of Technology, Guangzhou 510006, Guangdong, China

5 Shanxi Xintai Iron and Steel Co., Ltd., Jiexiu 032000, People's Republic of China

6 Foshan Water and Environmental Protection Co., Ltd., Foshan 528000, China

7 School of Environmental Science and Engineering, Guangdong University of Technology, Guangzhou 510006, China

GGBFS has been widely used as a supplementary cementitious material to partially replace cement [4–6]; however, a gap still exists between GGBFS production and utilization. Zhu et al. [1] reported that in China, only 80–100 million tons of GGBFS are used. Considering the inadequate use and recycling of this solid waste, technologies for its effective utilization are needed. Geopolymerization has been considered as a potential alternative technology for the utilization of this solid waste because of its ability to convert aluminosilicate sources into green and sustainable binders.

Generally, geopolymerization can be described as follows: (1) the dissolution of aluminosilicate in an alkali/acid activator and the formation of tetrahedral [AlO_4] and [SiO_4] units; (2) the reorganization and diffusion of tetrahedral [AlO_4] and [SiO_4] units; (3) polycondensation to form an aluminosilicate gel phase; and (4) the hardening of the aluminosilicate gel [7]. Finally, a geopolymer is formed as an inorganic polymeric material with a unique three-dimensional network structure. The geopolymer exhibits high durability, good chemical resistance, and excellent mechanical properties, making it highly useful in applications, such as heavy metal immobilization, infrastructure construction, and composite manufacturing [8–10].

Studies have reported that the CO_2 footprint of concrete prepared with geopolymer is 40–80% less than that of concrete prepared with 100% ordinary Portland cement [11–13]. Hence, geopolymers are regarded as eco-friendly. Moreover, raw materials with reactive silica and alumina, such as metakaolin, fly ash (FA), and GGBFS, can be used as the precursors for geopolymer synthesis [9, 14–17]. Studies have confirmed that GGBFS has high reactivity with alkaline solutions and that geopolymers prepared via the alkali-activation of GGBFS exhibit excellent mechanical properties [1–3, 18, 19]. Aziz et al. [18] studied the strength development of a GGBFS-based geopolymer (Gp) and found that a Gp with a solid-to-liquid ratio of 3.0 exhibited a high compressive strength of 168.7 MPa after 28 days of curing. Jang et al. [20] and Deb et al. [21] investigated the properties of FA/GGBFS-based geopolymer with different FA/GGBFS ratios. The increased concentration of GGBFS led to a denser microstructure or the co-existence of geopolymer gel and C-(A)-S-H (C: Ca; A: Al; S: Si; H: H_2O) and thus an increase in compressive strength [22].

However, the quasi-brittleness and low flexural strength of Gp usually limit their wide application [23–25]. The incorporation of fibers into the geopolymer may be a feasible way to overcome the geopolymer brittleness, because fibers can provide a good resistance to cracking and increase the fracture toughness of the brittle matrix [26, 27]. For instance, Long et al. [28] found that Gp reinforced with steel fibers showed a high storage modulus. Shoaei et al. [29] confirmed that the incorporation of polypropylene (PP) fibers, glass fibers, and basalt fibers improved the compressive and flexural strengths of the Gp. The geopolymer composite with 0.5 vol% of PP fibers exhibited 14% higher compressive strength than the control geopolymer after 28 days of curing. Besides, the addition of 0.5 vol% of glass fibers and 1 vol% of basalt fibers enhanced the 28-day compressive strength by 37% and 26%, respectively. Moreover, the geopolymer reinforced with 0.5 vol% of PP fibers, 1 vol% of glass fibers, and 1 vol% of basalt fibers exhibited 44%, 28%, and 33% higher flexural strengths than the control geopolymer.

The above results also reflected that different types of short fibers, including steel fiber, PP fiber, polyvinyl alcohol (PVA) fiber, polyethylene (PE) fiber, glass fiber, and basalt fiber, have different reinforcement effects on the mechanical properties of Gp [30–34]. Among these fibers, the PVA fiber is considered a suitable reinforcement fiber because of its outstanding alkali and acid resistance [35]. Mastali et al. [36] have also proved that Gp reinforced with PVA fibers outperformed basalt and PP fibers. Adding PVA fiber can help minimize the shortcomings of geopolymer, such as drying shrinkage and brittleness. Besides, it was reported that the integrity of geopolymer under impact loading at similar strain rates, the freeze–thaw, and carbonation resistance are improved by adding PVA fiber [37–39]. For example, the fiber-free geopolymer was destroyed in 50 freeze–thaw cycles while geopolymer incorporated with 2.0 vol% PVA fibers can withstand 175 freeze–thaw cycles. This can be explained as the mechanical interlocking effect of PVA fiber and reduced in porosity of geopolymer composite [38]. On the other hand, due to the hydrophilicity and low density of PVA fiber, incorporation of PVA fiber into geopolymer caused a decrease in the density, flowability, workability, consistency, sorptivity, and chloride penetration [40, 41].

Therefore, PVA fiber can pose positive and negative roles on geopolymer, depending on many factors, including the content, the length, and so on. With the regard to the fiber content, it should note that a high dosage of fiber can cause a clumping effect [42]. Furthermore, overdose PVA fiber content deteriorated the structure of geopolymer matrix near the PVA fiber, which became sparser [37]. Xu et al. [43] found that the compressive and flexural strengths of GGBFS-steel slag-based geopolymer reduced after incorporation of 0.4 vol% PVA fiber while adding 0.2 vol% PVA fibers enhanced the compressive and flexural strengths by 13.6% and 20.6%, respectively. However, previous studies also revealed that the optimal content of PVA fiber in geopolymer is different [44, 45], which needs to further research. Investigations performed by Abdollahnejad et al. [44] indicated that the a maximum compressive strength of GGBFS-based geopolymer was obtained after incorporating 1.0 wt% PVA while

Sun and Wu [45] reported that the optimal PVA fiber content for FA-based geopolymer was estimated to be 1.0 vol%.

Thus far, most of the studies related to PVA fiber-reinforced geopolymers more focused on blended (with FA, MK, ceramic, steel slag, and so on) or FA-based geopolymer than Gp [25, 41]. Besides, PVA fiber-reinforced Gp (FRGp) mortar or concrete was also presented in numerous studies, but scholars mostly concentrated on the mechanical properties rather than the influences of microstructure on the mechanical properties of the Gp. For example, although Kadhim et al. [40] referred to the durability of PVA FRGp mortars after incorporation of aggregate, the effect of fiber content and microstructure were not considered. Lee et al. [46] reinforced a GGBFS-based mortar with 2 vol% of PVA fiber and found that the tensile strength of the mortars was increased by 4.7%; however, how the microstructure affects the mechanical properties, and the mechanism of the improvement tensile strength were still unknown. Nevertheless, the limited studies concentrated on the mechanical properties rather than microstructure of PVA fiber-reinforced Gp. Choi et al. [34] found that hybrid PE–PVA fibers improved mechanical properties and autogenous healing of a Gp; similarly, this study did not focus on the microstructure of Gp. However, the development of mechanical properties of Gp is highly affected by microstructure. Systematic investigation about the influence of mechanical properties and microstructure of FRGp is neglected. In order to promote the application of GGBFS in the practice, it is necessary to clarify the relationship between the microstructure and mechanical properties of FRGp.

To elucidate the relationship between the mechanical properties and microstructure, the Gp was reinforced with PVA fibers. The mechanical properties of Gp and FRGp were characterized via compressive strength and flexural strength tests. The chemical compositions of Gp and FRGp were determined through several techniques, including Fourier-transform infrared (FTIR) spectroscopy and X-ray diffraction (XRD). The microstructural features and pore structures of Gp and FRGp were characterized via scanning electron microscopy/Energy-dispersive X-ray detector (SEM/EDX), and mercury intrusion porosimetry (MIP), respectively.

Experiment

Materials

GGBFS was supplied by Shanxi Antai Group Co., Ltd. The chemical compositions of GGBFS, determined via X-ray fluorescence (XRF), are listed in Table 1. GGBFS was mainly composed of calcium oxide (CaO), silica (SiO_2), aluminum oxide (Al_2O_3), and magnesium oxide (MgO). The XRD pattern of GGBFS (Fig. 1a) featured a broad hump centered at around $2\theta = 30.0°$, indicating that it was mainly composed of a glassy phase. Moreover, the diffraction reflections at about 29.4°, 36.0°, 39.4°, 43.1°, 47.5°, and 48.5° (2θ) were

Table 1 Oxides constituent of GGBFS and loss of ignition in percentage by weight

	CaO	SiO_2	Al_2O_3	MgO	Na_2O	MnO	K_2O	TiO_2	SO_3	L.O.I
GGBFS	38.57	30.00	15.01	9.35	0.43	0.51	0.29	0.64	3.48	0.17

L.O.I loss on ignition

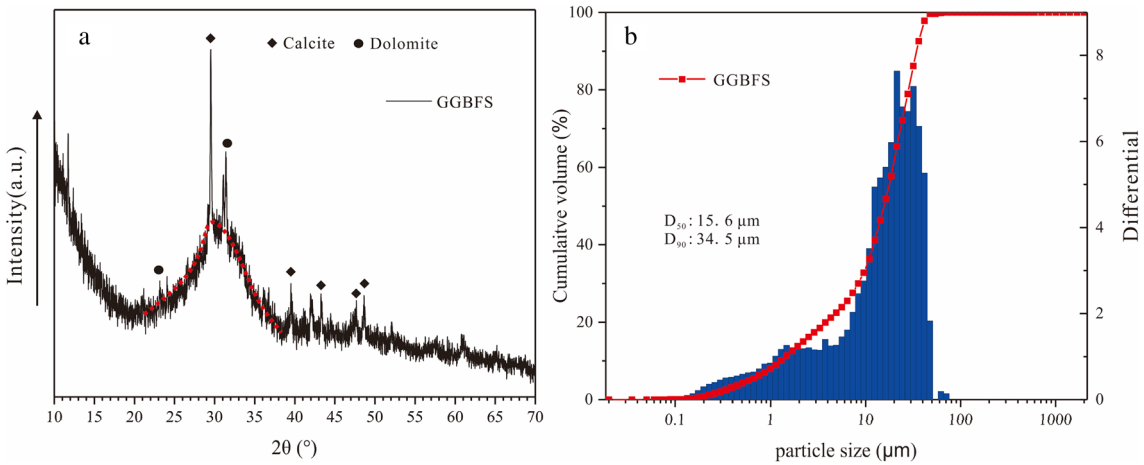

Fig. 1 **a** XRD pattern of GGBFS; **b** particle size distribution of GGBFS

Table 2 The properties of PVA fibers

Length (mm)	Nominal diameter (μm)	Density (g/cm^3)	Elastic modulus (GPa)	Tensile strength (MPa)	Broken elongation (%)
3	15.09	1.29	40	1830	6.9

Table 3 The properties of sodium silicate

Appearance	Modulus	Baume degree (Be)	Na_2O (wt%)	SiO_2 (wt%)	Density (g/cm^3)
Colorless and transparent	3.31	40	8.73	28.01	1.387

indexed to calcite while dolomite can be recognized at about 23.2° and 31.4° (2θ). The presence of calcite and dolomite indicated that the GGBFS was carbonated to some extent. The particle size distribution of GGBFS is shown in Fig. 1b. The D_{50} of GGBFS was 15.64 μm. PVA fibers were obtained from commercial suppliers. The physical properties of the PVA fibers used in this study are presented in Table 2. Both the GGBFS and PVA fibers were directly used without any treatment.

Figure 2 shows the photographs and SEM images of the raw materials used to prepare Gp and FRGp, including GGBFS and PVA fibers. GGBFS occurred as a gray–white irregular solid (Fig. 2a, c). The PVA fibers easily agglomerated (Fig. 2b), and the texture exhibited some longitudinal striations (Fig. 2d).

The properties of commercial sodium silicate, with a modulus (the molar ratio of SiO_2/Na_2O) of 3.31, are shown in Table 3. The commercial sodium silicate was mixed with chemical-grade sodium hydroxide pellets (purity ≥ 97%) to prepare an alkaline activator solution with a modulus of 1.5. This composition was selected based on preliminary experiments, which favored the development of mechanical properties. Ultrapure water was added to the solution to adjust the concentration $(m(SiO_2)+m(SiO_2))/(m(SiO_2)+m(SiO_2)+m(water))$ of 35%. The solutions were stored at room temperature for 1 day before use.

Table 4 Mix compositions of Gp and FRGp

Mix no	GGBFS (wt%)	PVA Fibers (wt%)	Liquid/solid ratio
Gp	100.0	0.0	0.5
Gp-0.5%PVA	99.5	0.5	0.5
Gp-1.0%PVA	99.0	1.0	0.5
Gp-2.0%PVA	98.0	2.0	0.5

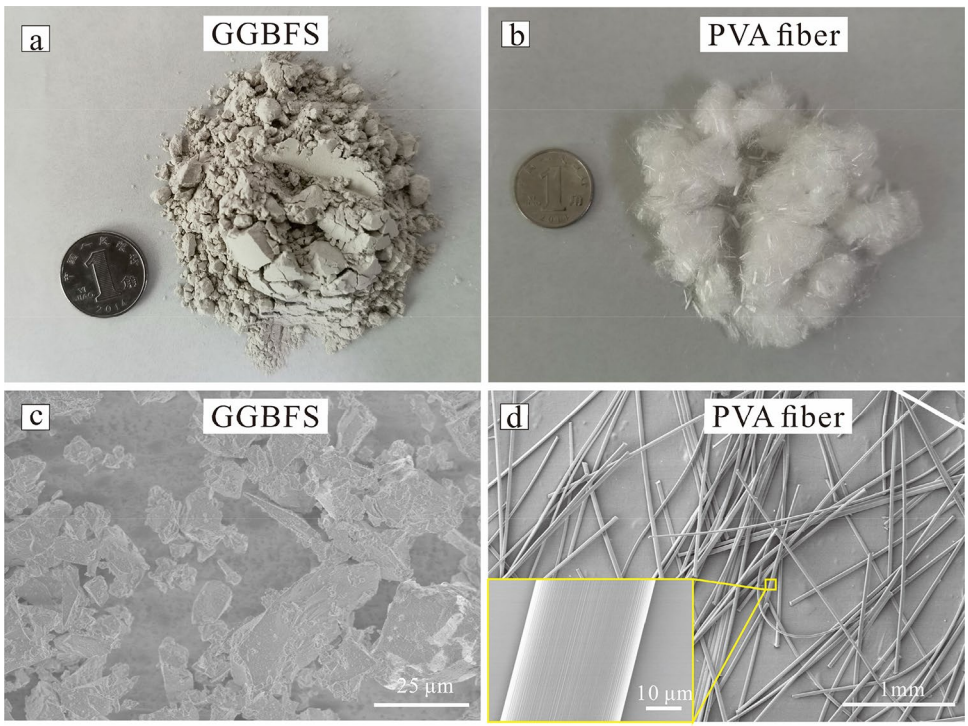

Fig. 2 Photographs of GGBFS (**a**) and PVA fibers (**b**); SEM micrographs of GGBFS (**c**) and PVA fibers (**d**)

Mixture design and preparation of geopolymer

The mix compositions for preparing Gp and FRGp are summarized in Table 4. The GGBFS was evenly mixed with PVA fibers in a 5-L mortar mixer (Wuxi Jianye Instrument, China) for approximately 10 min at a low speed (140 ± 5 r/min). The activator solution was added to the mixer with a liquid/solid ratio of 0.5. The resulting geopolymeric paste was then poured into 20 × 20 × 20 mm^3 silicon molds or 40 × 40 × 160 mm^3 plastic molds and vibrated for 1 min to remove the entrained air bubbles. All specimens were cured at ambient temperature and demolded after curing for 24 h. Finally, the cured specimens were sealed in plastic bags and then aged at ambient temperature. The non-fibrous matrix specimen was denoted as Gp and the fiber-reinforced geopolymer was denoted as "Gp-xPVA"; for example, Gp-1.0%PVA represents Gp reinforced with 1.0 wt% PVA fibers.

Isopropanol (purity ≥ 99.5%) was used to stop hydration for Gp and FRGp specimens under 28 days of curing, and the solvent was changed after 2 days. The specimens were stored in isopropanol for at least 4 days and then vacuum-dried for a minimum period of 3 days before spectroscopic and microscopic tests.

Characterization methods

The particle size distribution of GGBFS was measured using a JL-1177 laser particle size analyzer.

The chemical compositions of GGBFS were determined via XRF spectrometry using a wavelength-dispersive sequential scanning spectrometer (Shimadzu XRF-1800).

The mechanical properties (compressive and flexural strengths) of Gp and FRGp specimens cured at ambient temperature and of ages 7, 14, and 28 days were determined using a compression resistance tester (YAW-300D, Schlikör, China), at a loading rate of 500 N/s.

The FTIR spectra of Gp and FRGp specimens in the range of 4000–400 cm^{-1} were recorded using a Bruker Vertex 70V spectrometer (Karlsruhe, Germany). Approximately 0.8 mg of the specimen powder with 80 mg potassium bromide (KBr) was mixed and pressed into a pellet. Over 64 scans were collected for each measurement at a resolution of 4 cm^{-1}.

The powder XRD patterns of the Gp and FRGp were taken in the range of 3°–70° (2θ) on a Bruker D8 Advance diffractometer (Mannheim, Germany) with Ni filter and Cu$K\alpha$ radiation ($\lambda = 0.154$ nm). The generator voltage and current were set to 40 kV and 40 mA, respectively. The scan rate was 10°(2θ)/min, and JADE software was used for analysis.

The SEM images and EDX spectroscopy were obtained using the SU8010 field-emission scanning electron microscope (Hitachi, Japan), with an accelerating voltage of 1.5 and 15 kV, respectively.

The total porosity and critical pore size of Gp and FRGp specimens at 28 days were determined using MicroActive Autopore V 9600. The intrusion pressure ranged from 0.10 to 61,000.00 psia, and the contact angle was set to 130°.

Results and discussion

Mechanical properties and failure mode

Compressive strength and flexural strength

The compressive strengths of FRGp with different PVA fiber contents cured at 7, 14, and 28 days are shown in Fig. 3a. The addition of PVA fibers reduced the compressive strength. Little differences in compressive strength existed between Gp-0.5%PVA and Gp-1.0%PVA. The 7-, 14-, and

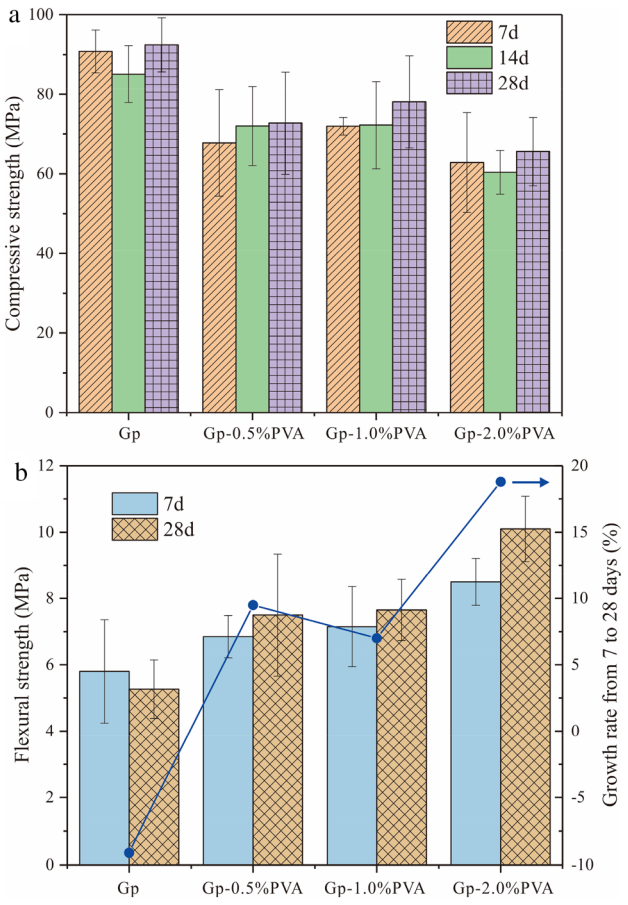

Fig. 3 Mechanical properties of of Gp and FRGps: **a** compressive strength; **b** flexural strength and growth rate of flexural strength from 7 to 28 days

28-day compressive strengths of Gp-1.0%PVA (71.9, 76.3, and 78.1 MPa, respectively) were lower than those of Gp (90.8, 85.1, and 92.4 MPa, respectively). However, the Gp with 2.0wt% of PVA fiber exhibited a more considerable difference in compressive strength: the 7-, 14-, and 28-day compressive strengths of Gp-2.0%PVA were 57.3, 62.6, and 68.0 MPa, 36.9%, 26.4%, and 26.4% lower than those of Gp, respectively. Other studies have reported such a weak effect on compressive strength [47, 48]. Zhong et al. [49] reported that FA/GGBFS-based geopolymer with 1.5 vol% and 2.0 vol% of PVA exhibited approximately 14.5% and 24.9% lower compressive strength than the fiber-free geopolymer, attributable to the entrapment of more air in the interfaces of FRGp [50].

The 7- and 28-day flexural strengths and the growth rate from 7 to 28 days of all specimens are illustrated in Fig. 3b. The flexural strengths of all specimens (except specimen Gp) slightly increased with increasing curing time from 7 to 28 days, owing to further geopolymerization. Incorporating the PVA fibers into Gp significantly increased its flexural strength. Gp with 0.5, 1.0, and 2.0 wt% of PVA fibers exhibited 42.3%, 45.2%, and 91.7% higher flexural strength than PVA-free Gp after 28 days of curing. Besides, with the increase of curing time, the growth rate of flexural strength of Gp decreased by 9.1% while those of Gp-0.5%PVA and Gp-1.0%PVA were similar (9.5% and 7.0%). When the content of PVA fiber increased to 2.0 wt%, an obvious growth rate of 18.8% was achieved.

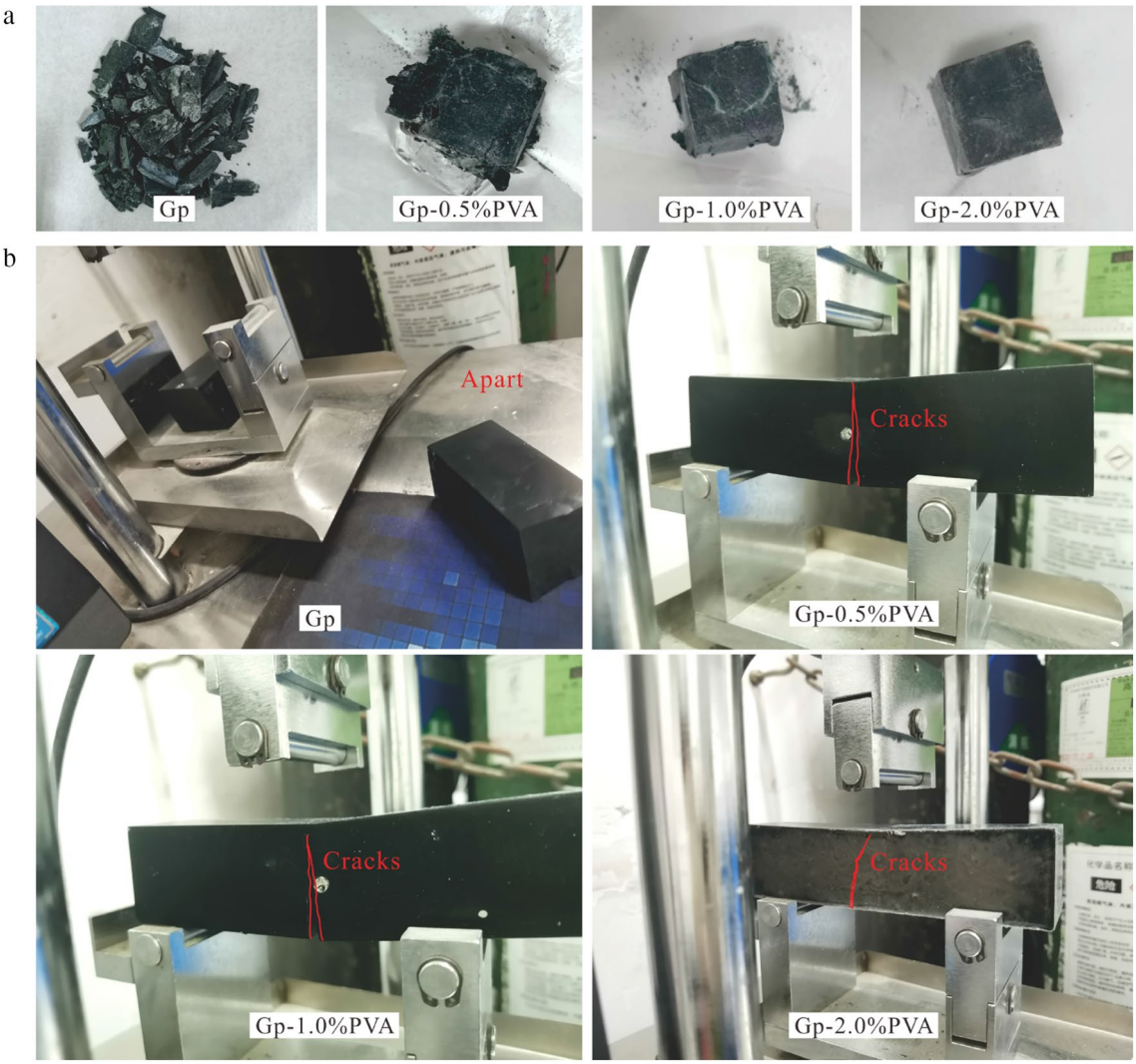

Fig. 4 Failure mode for Gp and FRGp after the **a** compressive and **b** flexural strength tests

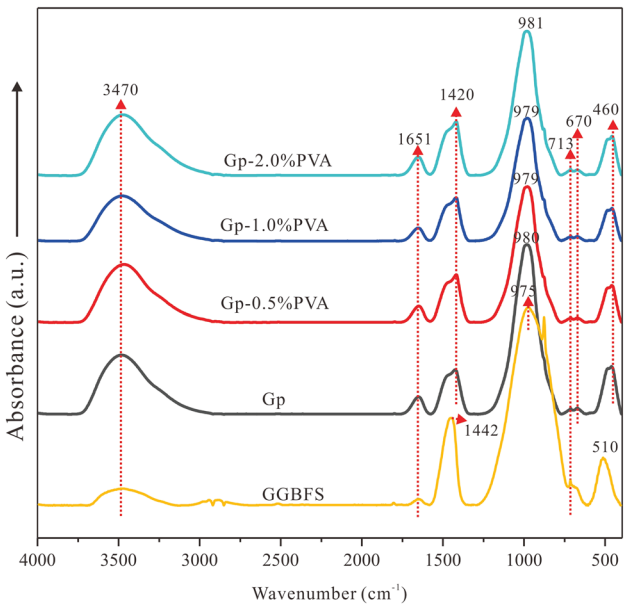

Fig. 5 FTIR spectra of GGBFS, Gp and FRGp specimens

Failure mode

The failure modes of specimens are shown in Fig. 4. Compared with Gp, the inclusion of PVA fibers into the geopolymer matrix altered the compression failure mode from highly brittle to relatively ductile (Fig. 4a). Gp exhibited a typical brittle failure with a high degree of matrix fragmentation. The FRGps with PVA fibers relatively preserved the original cubic shape of the specimen, although the ultimate load was reached, owing to the high elastic modulus and the bridging effect of the PVA fibers [51]. Besides, the integrity of FRGps increased after the addition of more fibers, demonstrating that more fibers can better confine crack propagation [52, 53] and more efficiently improve the ductile behavior of the geopolymer [54].

Similarly, after the flexural strength test, Gp was broken into two parts, whereas FRGps showed some cracks but did not break from the middle (Fig. 4b). This demonstrates that the PVA fibers in the geopolymer actively prevented a catastrophic failure.

Composition and microstructure of specimens

FTIR results

The FTIR spectrum of GGBFS shown in Fig. 5 is different from those geopolymer specimens. However, the FTIR spectra of Gp, and FRGp (Fig. 5) showed no considerable difference, indicating that the addition of PVA fibers did not significantly alter the structure at an atomic level for Gp and FRGp. Therefore, the PVA fibers were connected to the geopolymer matrix mainly through physical interaction.

The spectra featured absorption peaks at approximately 3470 cm^{-1} and 1651 cm^{-1}, corresponding to the stretching vibration of O–H and the bending vibration of H–O-H, respectively [55, 56]. The bands at 1420 cm^{-1} corresponded to the symmetric stretching vibration of O-C-O bonds [57, 58], whereas the band at 713 cm^{-1} was related to the out-of-plane bending vibrations of CO_3^{2-} [59], confirming the carbonation of GGBFS. The strongest band, located at 975 cm^{-1} in GGBFS and assigned to Si–O–T (where T is Si or Al), shifted to higher wavenumber (979–981 cm^{-1}) after geopolymerization, revealing the dissolution of the initial solid material into the strongly alkaline aqueous solution and the formation of a new aluminosilicate phase [60–62]. Besides, an absorption band at 670 cm^{-1} appeared after geopolymerization, and this band was related to the Al–O vibrations of the AlO_4 groups, demonstrating the formation of a new amorphous phase after geopolymerization [63]. The band at 460–510 cm^{-1} was assigned to the Si–O–Si asymmetric tensile vibration [63].

XRD results

No considerable difference existed between the XRD patterns of Gp and FRGp specimens after 28 days of curing (Fig. 6), reflecting that PVA fibers addition to Gp did not alter the mineral composition of the matrix.

The main crystalline phases were calcium silicate hydrate (C–S–H), calcite ($CaCO_3$, PDF#85-0849), and dolomite ($CaMg(CO_3)_2$, PDF#79-1344), and all specimens exhibited a broad amorphous reflection between 20° and 40° (2θ), indicating the presence of an amorphous phase [64]. Dolomite can be observed at 23.2° and 31.4°(2θ) while reflection at around 29.4° (2θ) was assigned to C-S–H crystal or calcite. The intensity of the reflection at 29.4° (2θ)

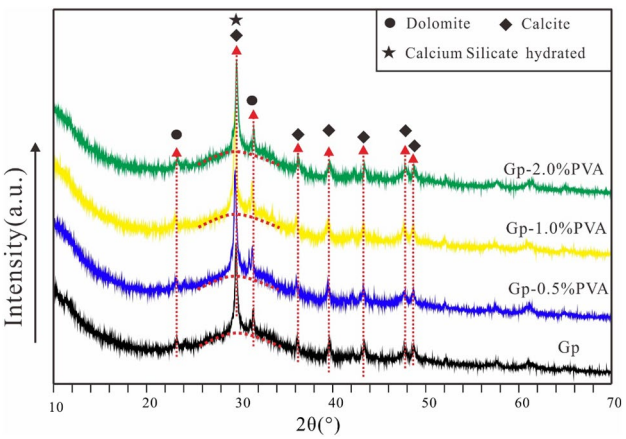

Fig. 6 XRD patterns of Gp and FRGp specimens

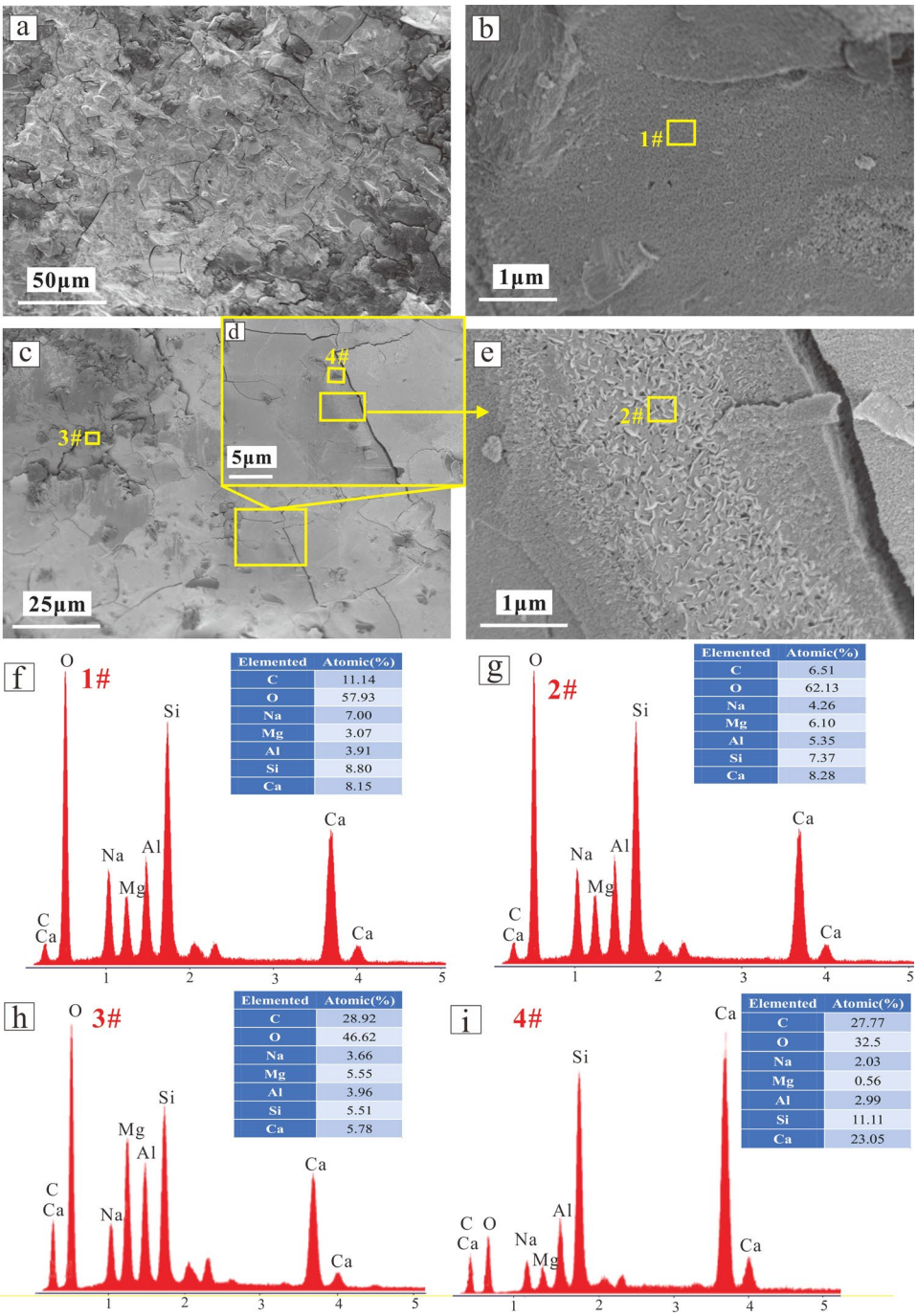

Fig. 7 SEM images of the Gp specimen: **a** homogeneous matrix; **b** matrix at high magnification; **c** and **d** crack in matrix; **e** matrix at high magnification. **f–i** EDX results of the matrix indicated in (**b**), (**c**), and (**e**)

should be reduced as calcite can react with alkali activators [65]. However, the intensity of this reflection was increased compared with that of GGBFS (Fig. 1a), which was mainly due to the formation of C–S–H crystal. Moreover, except the reflection at around 29.4 (2θ), calcite can also be recognized at 36.0°, 39.4°, 43.1°, 47.5°, and 48.5° (2θ).

SEM results

Figures 7, and 8 demonstrate the SEM/EDX images of the fracture surfaces of 28-day Gp and Gp-2.0%PVA after the test for mechanical properties. The SEM images were used for understanding the morphology of geopolymer specimens while EDX results were based on the atomic (%) to confirm the composition.

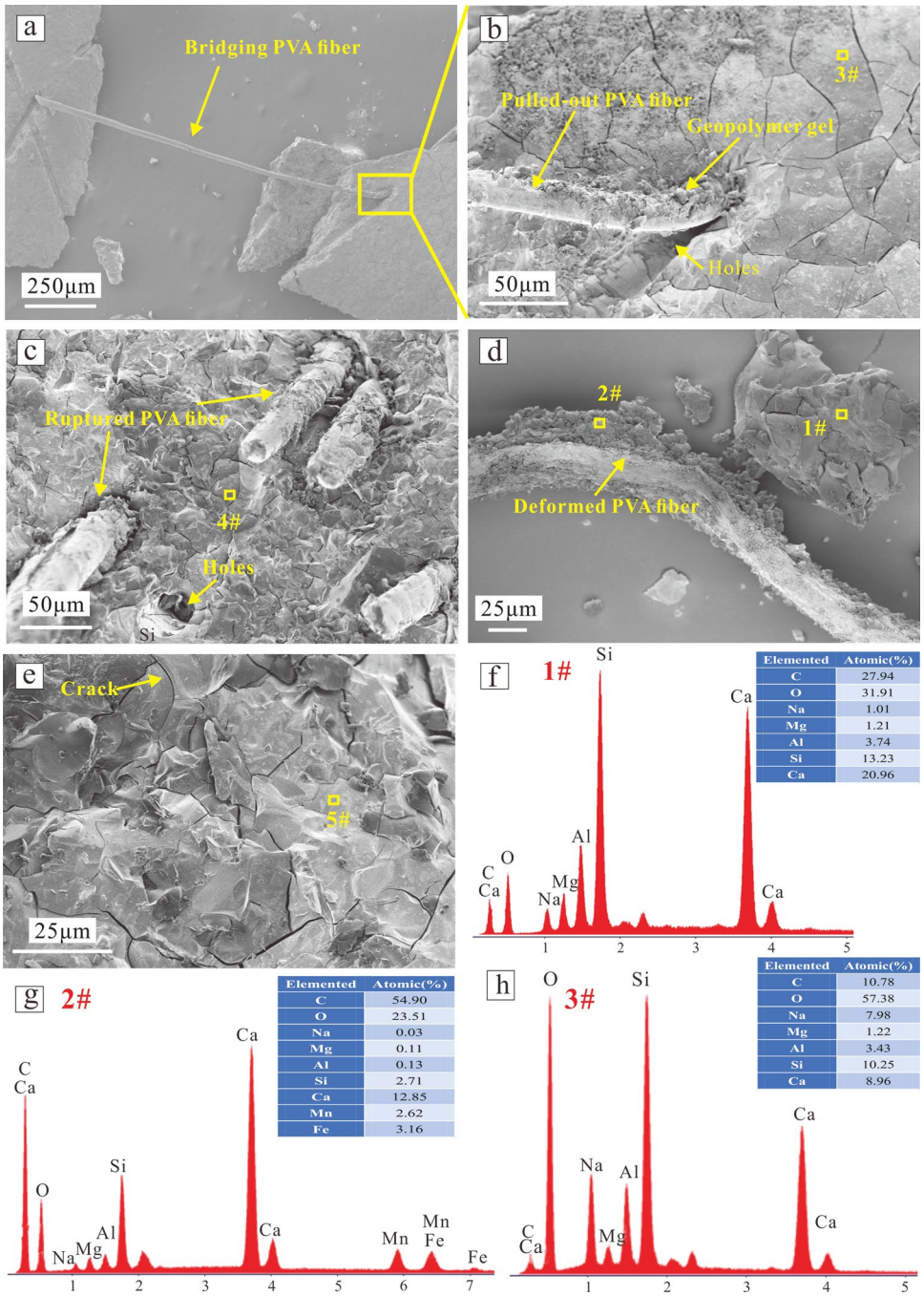

Fig. 8 SEM images of the Gp-2.0% PVA specimen: **a** the bridging effect of PVA fibers; **b** pulled-out PVA fibers and holes; **c** the non-uniform dispersion of PVA fibers; **d** deformed PVA fibers; **e** crack in matrix. **f–h** EDX result of the matrix indicated in (**b**) and (**d**)

The SEM images of Gp (Fig. 7a) showed that the matrix was dense and homogeneous. As displayed in Fig. 7b, SEM images of Gp showed a worm-like porous microstructure and EDX result (Fig. 7f) proved that those phases were geopolymer gel for its high content of Na, O, Ca, and Si. Cracks were distributed inside the specimen (Fig. 7c, d), resulting from the destruction of structure during compressive strength test. It can be observed that many platy-like particles on the Gp surface (Fig. 7e), and the EDX result (Fig. 7g) indicated that these particles are mainly C/N-(A)-S-H, whose composition were mainly comprised of O, Na, Si, Al, Ca, and traces of Mg. Besides, those particles connected together to form a homogenous matrix, indicating that it should not be a GGBFS particle. However, there were many unreacted particles found in the matrix. EDX shown in Fig. 7h indicated the existence of calcite or dolomite for high content of C, O, Mg, and Ca while Fig. 7i reflected the unreacted GGBFS for its high content of C, Si, Ca, and relative low O content compared with other location's.

As shown in Fig. 8a, the PVA fibers functioned as a bridge connecting the geopolymer matrix even in the presence of macro-cracks. Longitudinal striations on the PVA fibers surfaces increased the adhesion of the matrix with the fibers [46]. Besides, it also indicated that the alkali activator solution did not significantly degrade the PVA fibers, thereby preserving their role. Moreover, most of the PVA fibers were covered by the geopolymer gel, indicating a strong adhesion between the geopolymer gel and fibers (Figs. 8b, c). The fiber failure mode is strongly influenced by the bond strength between fibers and matrix. Fiber pulled-out occurred in the presence of a weak interfacial transition zone (ITZ), whereas a strong ITZ resulted in the fiber ruptured [66]. It can also be observed some ruptured PVA fibers and holes resulting from pulling-out of PVA fibers, presented in the geopolymer matrix. And the pulled-out PVA fiber has undergone a certain deformation (Fig. 8d). This reflects that both fiber ruptured and fiber pulled-out occurred for PVA fibers. The cracks were distributed in the matrix of specimen Gp-2.0%PVA (Fig. 8e), with a crack width of less than 0.87 µm. Furthermore, unlike Fig. 8c, e showed no PVA fibers, indicating that the PVA fibers were not well dispersed. Similarly, EDX displayed in Fig. 8f–h implied the co-existence of the GGBFS (Fig. 8f), calcite and dolomite (Fig. 8g), and C/N-(A)-S-H geopolymer gel (Fig. 8h). More EDX data of Gp-2.0%PVA were provided in Supplementary Material (Fig. S1).

More SEM images of Gp-0.5%PVA and Gp-1.0%PVA were provided in Fig. S2 and Fig. S3 (in Supplementary Material), and similar EDX data of Gp-0.5%PVA and Gp-1.0%PVA can be found in Fig. S4 (in Supplementary Material). These images indicated that the matrix of FRGp was inhomogeneous even in the same specimen, namely, geopolymer gel, calcite and dolomite, and GGBFS were co-existence. Combining the FTIR and XRD results, it can be concluded that the addition of PVA fiber did not change much the composition of geopolymer.

Pore structure

Figure 9 displays the total porosity and the critical pore size of Gp and Gp-2.0%PVA after 28 days of curing. The total porosity of the Gp with 2 wt% of PVA fibers (7.6%) was greater than that of the PVA-free Gp (4.0%) (Fig. 9a). The critical pore size corresponds to the peak of the differential pore volume curve, and shows the size at the maximum volume intrusion. After the incorporation of PVA fibers, the critical pore size of specimen Gp-2.0%PVA became larger than that of Gp. The Gp specimen possessed a large volume of pores with diameters ranging at 4×10^3–8×10^3 nm, whereas specimen Gp-2.0%PVA exhibited a wide pore diameter range of 1×10^3–200×10^3 nm (Fig. 9b). The increase in total porosity and pore size is attributable to the formation of an ITZ between the matrix and the PVA fibers, which introduced a large number of mesopores around the fibers [28, 29, 67], as confirmed by SEM images (Fig. 8c, Fig. S2d, and Fig. S3c). The occurrence of mesopores consequently reduced the compressive strength, as discussed in "Compressive strength and flexural strength". However, the function of PVA fibers for preventing of crack propagation and energy absorption can mitigate the detrimental effect resulting from the increase in total porosity and the enlargement of pore size. Therefore, the flexural strength increased, rather than decreased.

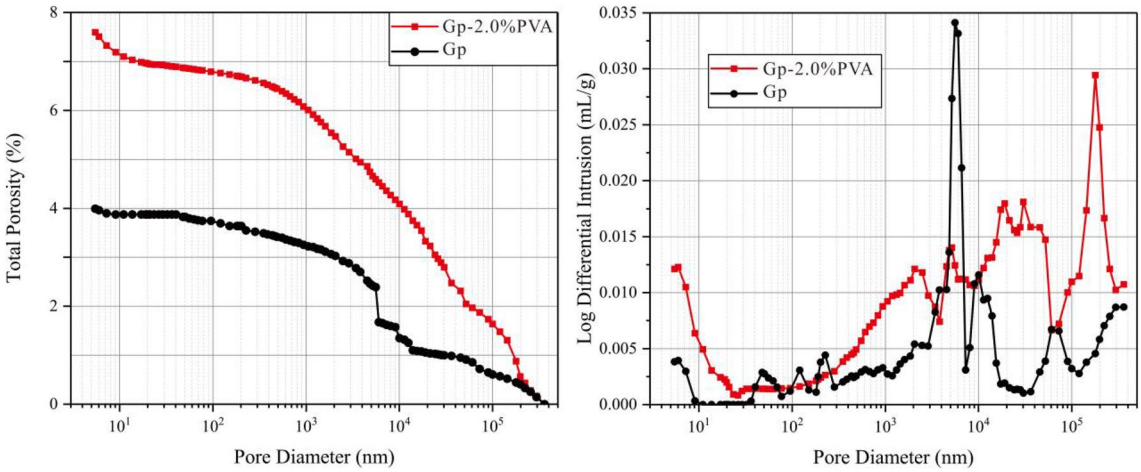

Fig. 9 MIP curves of Gp and Gp-2.0%PVA: **a** total porosity and **b** differential intrusion volume

Summary and conclusion

In this study, the effects of PVA fiber content on the compressive strength, flexural strength, composition, morphology, and pore structure of the Gp and FRGp were evaluated. And the relationship between the mechanical properties and microstructure of Gp and FRGp was systematically investigated through a combination of microscopic and spectroscopic techniques. Based on the experimental results and analytical studies, the main conclusion can be drawn as follows:

(1) The incorporation of PVA fibers into Gp reduced its compressive strength but increased its flexural strength. The increase in total porosity and pore size due to fibers addition was detrimental to the mechanical properties of the FRGps. However, the PVA fibers confined crack propagation and absorbed energy, thereby mitigating the detrimental effect and increasing flexural strength. With increasing fiber content, the effect on the FRGp's mechanical properties became more significant. The Gp with 2.0 wt% of PVA fibers exhibited a lower compressive strength (68.0 MPa) than the PVA-free Gp (92.4 MPa) but 91.7% higher flexural strength after 28 days of curing. Besides, with the increasing curing time from 7 to 28 days, an obvious growth rate of 18.8% was achieved for this specimen.

(2) The PVA fibers strongly adhered to the geopolymer matrix via physical interaction and did not alter the mineral composition of the FRGps. Furthermore, the geopolymer failure mode was transformed from brittleness into ductile failure after PVA fibers incorporating, whereas the failure mode of the PVA fibers was fiber pulled-out and fiber ruptured.

In conclusion, the PVA fibers considerably influenced the microstructure of the as-obtained Gp and FRGp, consequently influencing their mechanical properties. However, only the relationship between mechanical properties and the microstructure of Gp and FRGp specimens was evaluated. Further properties dependent on microstructure, such as dynamic mechanical properties, physical properties, and durability (e.g., freeze–thaw performance), need to be studied for the application of geopolymers as building material in the construction field.

Supplementary Information The online version contains supplementary material available at https://doi.org/10.1007/s10163-023-01646-3.

Acknowledgements This work is supported by the National Natural Science Foundation of China (Grant Nos. 41972045 and 52161145405), Basic and Applied Basic Research Foundation of Guangdong Province (Grant No. 2021A1515110941), and the National Special Support for High-Level Personnel. This is contribution No. IS-3328 from GIGCAS.

Data availability The datasets generated and/or analyzed during the current study are available from the corresponding author on reasonable request.

References

1. Zhu X, Zhang M, Yang K, Yu L, Yang C (2020) Setting behaviours and early-age microstructures of alkali-activated ground granulated blast furnace slag (GGBS) from different regions in China. Cem Concr Compos 114:103782. https://doi.org/10.1016/j.cemconcomp.2020.103782
2. Carvalho S, Vernilli F, Almeida B, Oliveira M, Silva S (2018) Reducing environmental impacts: the use of basic oxygen furnace slag in portland cement. J Cleaner Prod 172:385–390. https://doi.org/10.1016/j.jclepro.2017.10.130
3. Abdalqader A, Jin F, Al-Tabbaa A (2016) Development of greener alkali-activated cement: utilisation of sodium carbonate for activating slag and fly ash mixtures. J Cleaner Prod 113:66–75. https://doi.org/10.1016/j.jclepro.2015.12.010
4. Yuksel I (2018) 12- Blast-furnace slag. In: Siddique R, Cachim P (eds) Waste and supplementary cementitious materials in concrete. Woodhead Publishing, pp 361–415
5. Li F, Liu L, Yang Z, Li S (2021) Physical and mechanical properties and micro characteristics of fly ash-based geopolymer paste incorporated with waste granulated blast furnace slag (GBFS) and functionalized multi-walled carbon nanotubes (MWCNTs). J Hazard Mater 401:123339. https://doi.org/10.1016/j.jhazmat.2020.123339
6. Crossin E (2015) The greenhouse gas implications of using ground granulated blast furnace slag as a cement substitute. J Clean Prod 95:101–108. https://doi.org/10.1016/j.jclepro.2015.02.082
7. Liew Y, Heah C, Mohd Mustafa A, Kamarudin H (2016) Structure and properties of clay-based geopolymer cements: a review. Prog Mater Sci 83:595–629. https://doi.org/10.1016/j.pmatsci.2016.08.002
8. Duxson P, Fernández-Jiménez A, Provis J, Lukey G, Palomo A, van Deventer J (2007) Geopolymer technology: the current state of the art. J Mater Sci 42(9):2917–2933. https://doi.org/10.1007/s10853-006-0637-z
9. Zhang B, Guo H, Yuan P, Li Y, Wang Q, Deng L, Liu D (2020) Geopolymerization of halloysite via alkali-activation: dependence of microstructures on precalcination. App Clay Sci 185:105375. https://doi.org/10.1016/j.clay.2019.105375
10. Bah A, Feng D, Kedjanyi E, Shen Z, Bah A, Li F (2022) Solidification of (Pb-Zn) mine tailings by fly ash-based geopolymer I: influence of alkali reagents ratio and curing condition on compressive strength. J Mater Cycles Waste Manage 24:351–363. https://doi.org/10.1007/s10163-021-01322-4
11. Turner L, Collins F (2013) Carbon dioxide equivalent (CO_2-e) emissions: a comparison between geopolymer and OPC cement concrete. Constr Build Mater 43:125–130. https://doi.org/10.1016/j.conbuildmat.2013.01.023
12. Ameri F, Shoaei P, Musaeei H, Zareei S, Ban C (2020) Partial replacement of copper slag with treated crumb rubber aggregates in alkali-activated slag mortar. Constr Build Mater 256:119468. https://doi.org/10.1016/j.conbuildmat.2020.119468
13. McLellan B, Williams R, Lay J, Riessen A, Corder G (2011) Costs and carbon emissions for geopolymer pastes in comparison to ordinary portland cement. J Cleaner Prod 19(9):1080–1090. https://doi.org/10.1016/j.jclepro.2011.02.010
14. Provis J (2018) Alkali-activated materials. Cem Concr Res 114:40–48. https://doi.org/10.1016/j.cemconres.2017.02.009

15. Zhang J, Li S, Li Z, Liu C, Gao Y (2020) Feasibility study of red mud for geopolymer preparation: effect of particle size fraction. J Mater Cycles Waste Manage 22:1328–1338. https://doi.org/10.1007/s10163-020-01023-4
16. Guo H, Zhang B, Deng L, Yuan P, Li M, Wang Q (2021) Preparation of high-performance silico-aluminophosphate geopolymers using fly ash and metakaolin as raw materials. App Clay Sci 204:10619. https://doi.org/10.1016/j.clay.2021.106019
17. Shoaei P, Musaeei H, Mirlohi F, Zamanabadi S, Ameri F, Bahrami N (2019) Waste ceramic powder-based geopolymer mortars: Effect of curing temperature and alkaline solution-to-binder ratio. Constr Build Mater 227:116686. https://doi.org/10.1016/j.conbuildmat.2019.116686
18. Aziz I, Abdullah M, Salleh M, Azimi E, Chaiprapa J, Sandu A (2020) Strength development of solely ground granulated blast furnace slag geopolymers. Constr Build Mater 250:118720. https://doi.org/10.1016/j.conbuildmat.2020.118720
19. Mahmood A, Noman M, Pechočiaková M, Amor N, Petrů M, Abdelkader M, Militký J, Sozcu S, Hassan S (2021) Geopolymers and fiber-reinforced concrete composites in civil engineering. Polymers 13:2099. https://doi.org/10.3390/polym13132099
20. Jang J, Lee N, Lee H (2014) Fresh and hardened properties of alkali-activated fly ash/slag pastes with superplasticizers. Constr Build Mater 50:169–176. https://doi.org/10.1016/j.conbuildmat.2013.09.048
21. Deb P, Nath P, Sarker P (2014) The effects of ground granulated blast-furnace slag blending with fly ash and activator content on the workability and strength properties of geopolymer concrete cured at ambient temperature. Mater Des 62:32–39. https://doi.org/10.1016/j.matdes.2014.05.001
22. Marjanović N, Komljenović M, Baščarević Z, Nikolić V, Petrović R (2015) Physical–mechanical and microstructural properties of alkali-activated fly ash–blast furnace slag blends. Ceram Int 41:1421–1435. https://doi.org/10.1016/j.ceramint.2014.09.075
23. Haddaji Y, Majdoubi H, Mansouri S, Tamraoui Y, Bouchti E, Manoun B, Oumam M, Hannache H (2021) Effect of synthetic fibers on the properties of geopolymers based on non-heat treated phosphate mine tailing. Mater Chem Phys 260:124147. https://doi.org/10.1016/j.matchemphys.2020.124147
24. Rashad A (2013) A comprehensive overview about the influence of different additives on the properties of alkali-activated slag–a guide for civil engineer. Constr Build Mater 47:29–55. https://doi.org/10.1016/j.conbuildmat.2013.04.011
25. Rashad A (2018) The effect of polypropylene, polyvinyl-alcohol, carbon and glass fibres on geopolymers properties. Mater Sci Technol 35:1–20. https://doi.org/10.1080/02670836.2018.1514096
26. Xu F, Deng X, Peng C, Zhu J, Chen J (2017) Mix design and flexural toughness of PVA fiber reinforced fly ash-geopolymer composites. Constr Build Mater 150:179–189. https://doi.org/10.1016/j.conbuildmat.2017.05.172
27. Huang Y, Tan J, Xuan X, Wei S, Liu L, Yu S, Zheng G (2022) Durability of plant fiber reinforced alkali activated composites. Constr Build Mater 314:125501. https://doi.org/10.1016/j.conbuildmat.2021.125501
28. Long W, Wu Z, Khayat K, Wei J, Dong B, Xing F, Zhang J (2022) Design, dynamic performance and ecological efficiency of fiber-reinforced mortars with different binder systems: ordinary Portland cement, limestone calcined clay cement and alkali-activated slag. J Cleaner Prod 337:130478. https://doi.org/10.1016/j.jclepro.2022.130478
29. Shoaei P, Ghassemi P, Ameri F, Musaeei H, Ban C, Ozbakkaloglu T (2021) Comparative study on the effect of fiber type and content on the fire resistance of alkali-activated slag composites. Constr Build Mater 288:123136. https://doi.org/10.1016/j.conbuildmat.2021.123136
30. Huang Y, Tan J, Xuan X, Liu L, Zheng G (2021) Study on untreated and alkali treated rice straw reinforced geopolymer composites. Mater Chem Phys 262(2):124304. https://doi.org/10.1016/j.matchemphys.2021.124304
31. Xu Y, Xing G, Zhao J, Zhang Y (2021) The effect of polypropylene fiber with different length and dosage on the performance of alkali-activated slag mortar. Constr Build Mater 307:124978. https://doi.org/10.1016/j.conbuildmat.2021.124978
32. Luna-Galiano Y, Leiva C, Villegas R, Arroyo F, Vilches L, Fernández-Pereira C (2018) Carbon fiber waste incorporation in blast furnace slag geopolymer-composites. Mater Lett 233:1–3. https://doi.org/10.1016/j.matlet.2018.08.099
33. Alves L, Leklou N, Souza F, Barros S (2021) Assessment of the effect of fiber percentage in glass fiber reinforced slag-based geopolymer. J Asian Ceram Soc 9(3):1265–1274. https://doi.org/10.1080/21870764.2021.1966977
34. Choi J, Nguyễn H, Park S, Ranade R, Lee B (2021) Effects of fiber hybridization on mechanical properties and autogenous healing of alkali-activated slag-based composites. Constr Build Mater 310:125280. https://doi.org/10.1016/j.conbuildmat.2021.125280
35. Xu S, Malik M, Qi Z, Huang B, Li Q (2018) Sarkar M Influence of the PVA fibers and SiO_2 NPs on the structural properties of fly ash based sustainable geopolymer. Constr Build Mater 164:238–245. https://doi.org/10.1016/j.conbuildmat.2017.12.227
36. Mastali M, Kinnunen P, Isomoisio H, Karhu M, Illikainen M (2018) Mechanical and acoustic properties of fiber-reinforced alkali-activated slag foam concretes containing lightweight structural aggregates. Constr Build Mater 187:371–381. https://doi.org/10.1016/j.conbuildmat.2018.07.228
37. Xiao S, Liao S, Zhong G, Guo Y, Lin J, Xie Z, Song Y (2021) Dynamic properties of PVA short fiber reinforced low-calcium fly ash - slag geopolymer under an SHPB impact load. J build Eng 44:103220. https://doi.org/10.1016/j.jobe.2021.103220
38. Li F, Chen D, Lu Y, Zhang H, Li S (2022) Influence of mixed fibers on fly ash based geopolymer resistance against freeze-thaw cycles. J Non-Cryst Solids 584:121517. https://doi.org/10.1016/j.jnoncrysol.2022.121517
39. Li F, Chen D, Yang Z, Lu Y, Zhang H, Li S (2022) Effect of mixed fibers on fly ash-based geopolymer resistance against carbonation. Constr Biuld Mater 349:126394. https://doi.org/10.1016/j.conbuildmat.2022.126394
40. Kadhim S, Çevik A, Nis A, Bakbak D, Aljanabi M (2022) Mechanical behavior of fiber reinforced slag-based geopolymer mortars incorporating artificial lightweight aggregate exposed to elevated temperatures. Constr Biuld Mater 315:125766. https://doi.org/10.1016/j.conbuildmat.2021.125766
41. Deng Z, Yang Z, Bian J, Lin J, Long Z, Hong G, Yang Z, Ye Y (2022) Advantages and disadvantages of PVA-fibre-reinforced slag- and fly ash-blended geopolymer composites: Engineering properties and microstructure. Constr Biuld Mater 349:128690. https://doi.org/10.1016/j.conbuildmat.2022.128690
42. Ranjbar N, Talebian S, Mehrali M, Kuenzel C, Metselaar HSC, Jumaat MJ (2016) Mechanisms of interfacial bond in steel and polypropylene fiber reinforced geopolymer composites. Compos Sci Technol 122:73–81. https://doi.org/10.1016/j.compscitech.2015.11.009
43. Xu S, Wu C, Yue J, Xu Z (2022) Shrinkage and mechanical properties of fibre-reinforced blast furnace slag-steel slag-based geopolymer. adv civil eng. https://doi.org/10.1155/2022/8931401
44. Abdollahnejad Z, Mastali M, Luukkonen T, Kinnunen P, Illikainen M (2018) Fiber-reinforced one-part alkali-activated slag/ceramic binders. Ceram Int 44:8963–8967. https://doi.org/10.1016/j.ceramint.2018.02.097

45. Sun P, Wu H (2008) Transition from brittle to ductile behavior of fly ash using PVA fibers. Cem Concr Compos 30:29–36. https://doi.org/10.1016/j.cemconcomp.2007.05.008
46. Lee B, Cho C, Lim H, Song J, Yang K, Li V (2012) Strain hardening fiber reinforced alkali-activated mortar–a feasibility study. Constr Build Mater 37:15–20. https://doi.org/10.1016/j.conbuildmat.2012.06.007
47. Wang Y, Chan C, Leong S, Zhang M (2020) Engineering properties of strain hardening geopolymer composites with hybrid polyvinyl alcohol and recycled steel fibres. Constr Build Mater 261:120585. https://doi.org/10.1016/j.conbuildmat.2020.120585
48. Yu K, Ding Y, Zhang Y (2020) Size effects on tensile properties and compressive strength of engineered cementitious composites. Cem Concr Compos 113:103691. https://doi.org/10.1016/j.cemconcomp.2020.103691
49. Zhong H, Zhang M (2021) Effect of recycled tyre polymer fibre on engineering properties of sustainable strain hardening geopolymer composites. Cem Concr Compos 122:104167. https://doi.org/10.1016/j.cemconcomp.2021.104167
50. Guo X, Pan X (2018) Mechanical properties and mechanisms of fiber reinforced fly ash–steel slag based geopolymer mortar. Constr Build Mater 179:633–641. https://doi.org/10.1016/j.conbuildmat.2018.05.198
51. Guo L, Wu Y, Xu F, Song X, Ye J, Duan P, Zhang Z (2020) Sulfate resistance of hybrid fiber reinforced metakaolin geopolymer composites. Compos B 183:107689. https://doi.org/10.1016/j.compositesb.2019.107689
52. Nematollahi B, Sanjayan J, Shaikh F (2015) Tensile strain hardening behavior of PVA fiber-reinforced engineered geopolymer composite. J Mater Civ Eng. https://doi.org/10.1061/(ASCE)MT.1943-5533.0001242
53. Nematollahi B, Sanjayan J, Shaikh F (2016) Matrix design of strain hardening fiber reinforced engineered geopolymer composite. Compos B 89:253–265. https://doi.org/10.1016/j.compositesb.2015.11.039
54. Masi G, Rickard W, Bignozzi M, Riessen A (2015) The effect of organic and inorganic fibres on the mechanical and thermal properties of aluminate activated geopolymers. Compos B 76:218–228. https://doi.org/10.1016/j.compositesb.2015.02.023
55. Somna K, Jaturapitakkul C, Kajitvichyanukul P, Chindaprasirt P (2011) NaOH-activated ground fly ash geopolymer cured at ambient temperature. Fuel 90(6):2118–2124. https://doi.org/10.1016/j.fuel.2011.01.018
56. Assaedi H, Alomayri T, Shaikh F, Low I (2015) Characterisation of mechanical and thermal properties in flax fabric reinforced geopolymer composites. J Adv Ceram 4:272–281. https://doi.org/10.1007/s40145-015-0161-1
57. Aboulayt A, Riahi M, Touhami M, Hannache H, Gomina M, Moussa R (2017) Properties of metakaolin based geopolymer incorporating calcium carbonate. Adv Powder Technol 28(9):2393–2401. https://doi.org/10.1016/j.apt.2017.06.022
58. Nath S (2018) Geopolymerization behavior of ferrochrome slag and fly ash blends. Constr Build Mater 181:487–494. https://doi.org/10.1016/j.conbuildmat.2018.06.070
59. Ylmén R, Jäglid U, Steenari B, Panas I (2009) Early hydration and setting of Portland cement monitored by IR, SEM and Vicat techniques. Cem Concr Res 39(5):433–439. https://doi.org/10.1016/j.cemconres.2009.01.017
60. Maragkos I, Giannopoulou I, Panias D (2009) Synthesis of ferronickel slag-based geopolymers. Miner Eng 22(2):196–203. https://doi.org/10.1016/j.mineng.2008.07.003
61. Zhang B, Yuan P, Guo H, Deng L, Li Y, Li L, Wang Q, Liu D (2021) Effect of curing conditions on the microstructure and mechanical performance of geopolymers derived from nanosized tubular halloysite. Constr Build Mater 268:121186. https://doi.org/10.1016/j.conbuildmat.2020.121186
62. Li F, Yang Z, Zheng A, Li S (2021) Properties of modified engineered geopolymer composites incorporating multi-walled carbon nanotubes (MWCNTs) and granulated blast furnace slag(GBFS). Ceram Int 47:14244–14259. https://doi.org/10.1016/j.ceramint.2021.02.008
63. Sun X, Liu J, Qiu J, Wu P, Zhao Y (2021) Alkali activation of blast furnace slag using a carbonate-calcium carbide residue alkaline mixture to prepare cemented paste backfill. Constr Build Mater 320:126234. https://doi.org/10.1016/j.conbuildmat.2021.126234
64. Ismail I, Bernal S, Provis J, Nicolas R, Hamdan S, Deventer J (2014) Modification of phase evolution in alkali-activated blast furnace slag by the incorporation of fly ash. Cem Concr Compos 45:125–135. https://doi.org/10.1016/j.cemconcomp.2013.09.006
65. Zhang Y, Xiao R, Jiang X, Li W, Huang B (2020) Effect of particle size and curing temperature on mechanical and microstructural properties of waste glass-slag-based and waste glass-fly ash-based geopolymers. J Cleaner Prod 273(1):122970. https://doi.org/10.1016/j.jclepro.2020.122970
66. Li Z, Zhang Y, Zhou X (2005) Short fiber reinforced geopolymer composites manufactured by extrusion. J Mater Civ Eng 17(6):624–631. https://doi.org/10.1061/(ASCE)0899-1561(2005)17:6(624)
67. Abdollahnejad Z, Mastali M, Mastali M, Dalvand A (2017) Comparative study on the effects of recycled glass-fiber on drying shrinkage rate and mechanical properties of the self-compacting mortar and fly ash-slag geopolymer mortar. J Mater Civ Eng 29(8):04017076. https://doi.org/10.1061/(ASCE)MT.1943-5533.0001918